Low-Order Model for Detonation Velocity Suppression in Rotating Detonation Combustors

Provence Barnouin*, Eric Bach†, Christian Oliver Paschereit‡, and Myles D. Bohon§
Technische Universität Berlin, 10623 Berlin, Germany

Ephraim J. Gutmark¶
University of Cincinnati, Department of Aerospace Engineering, Cincinnati, OH 45220, USA

A Rotating Detonation Combustor (RDC) is a novel pressure gain combustion device, in which a detonation wave processes steadily around an annulus. It has been experimentally observed that detonation waves in the RDC propagate slower than the idealized Chapman-Jouguet (CJ) speed (as low as approximately 60%) and with lower than expected peak pressures. This work then attempts to develop a low-order model to identify the impact of non-ideal processes on these key detonation properties. Three mechanisms are incorporated: the buffer region created by non-premixed reactant injection, parasitic combustion of reactants, and suppression of the heat release through the detonation. While these sophisticated processes are only coarsely described by such a low-order model, it is shown that their effect results in a partial heat release that supports the detonation wave and can capture the deficit in detonation properties. One special aspect of this model is that it is designed to utilize relatively easily measured experimental data as inputs. This has the objective of providing rough, first order estimates of these more sophisticated processes than would otherwise be available by typical RDC combustor diagnostics. A parametric analysis is conducted for stable detonation runs on the RDC at TU Berlin. Convergence between predicted and experimental values show that a significant proportion of the heat release is lost in the buffer zone, undergoes parasitic combustion or is unable to contribute to the detonation heat release.

I. Introduction

Pressure Gain Combustion (PGC) technologies have the potential to significantly increase efficiency in power generation and propulsion applications. In comparison to constant pressure combustion, PGC is a process which results in a more effective conversion of the chemical energy stored in the fuel as both temperature and stagnation pressure of the product gas are increased. The Rotating Detonation Combustor (RDC) is a particularly studied form of PGC technology due to its simple geometric design. It consists of an annular gap where a detonation wave processes continuously through an unburned mixture, supplied by the fuel and oxidizer injectors. The detonation wave compresses and ignites the reactants, which then expand and accelerate axially down the annulus. Theoretically, the flow exiting the chamber has a net higher total pressure than the flow entering it. Thrust can then be derived from the raise in stagnation pressure.

While the RDC is relatively simple in design, experimental measurements of characteristic properties to a scale sufficient to resolve flow phenomena is difficult due to the harsh conditions and short time scales inside the annulus. Thus, numerous operating processes inside the RDC annulus remain to be understood. In particular, wave speeds measured experimentally are often much lower than those predicted by the Chapman-Jouguet (CJ) condition. Bach et al. found that inside a non-premixed RDC, the detonation wave often propagates at around 70-80% of the Chapman–Jouguet (CJ) velocity [1, 2]. These velocity and pressure deficits are often not captured in many computational fluid dynamic (CFD) simulations of RDCs. Klopsch et al. applied a two-dimensional, time-resolved reactive Euler solver to model the aforementioned RDC configuration and reported CJ velocities between 89% and 95% [3]. In a complimentary high-fidelity computation by Nassini, the predicted wave speed was 19% higher than the measured one at similar operating conditions [4]. The discrepancy between measured and computed wave speeds has also been observed on other RDC configurations by numerous studies [5–10].

*PhD Student, Chair of Pressure Gain Combustion, TU Berlin.
†Postdoctoral Researcher, Chair of Pressure Gain Combustion, TU Berlin, AIAA Student Member.
‡Professor, Chair of Fluid Dynamics, TU Berlin, AIAA Associate Fellow.
§Professor, Chair of Pressure Gain Combustion, TU Berlin, AIAA Member.
¶Distinguished Professor, Ohio Regents Eminent Scholar, UC, AIAA Fellow, TU Berlin, AIAA Associate Fellow.

There are multiple mechanisms that could reasonably contribute to the reduction in detonation wave speeds observed in experiments. These mechanisms could include non-ideal injection and mixing, exhaust gas dilution, deflagrative burning, heat loss, viscous processes and lateral relief [11]. Previous researchers have studied the effect of one or a combination of these mechanisms on detonation operation inside an RDC. In particular, several studies have examined the injection process and its resulting reactants dynamics. Rankin et al. studied injector dynamics using acetone planar laser induced fluorescence imaging in an optically accessible RDC and observed that fuel was not being injected into the annulus for approximately 20% of the cycle time after the passage of a detonation wave [12]. Although reactants were supplied continuously to the RDC, it is hypothesized that the high pressure generated by the detonation wave temporarily blocked fuel injection. In certain injector configurations, the high pressure was shown to also induce combustion product backflow into the supply plenum [8]. Furthermore, Chacon and Gamba performed OH* chemiluminescence imaging in a racetrack RDC and identified a region devoid of chemiluminescence between the recirculated products and fresh reactant mixture [5]. The authors attributed this to the presence of a fuel buffer region where chemical reactions cannot be sustained. In their configuration, the stiffer fuel injector recovered faster than the oxidizer injector generating a rich buffer region. The buffer zone thus represents a portion of reactants with local equivalence ratios that increasingly diverge from the nominal, global equivalence ratio and also thereby varies the local equivalence ratio ahead of the detonation, shifting the mixture leaner or richer depending on whether there is a higher injector pressure in the fuel or air injector, respectively. Injection is thus a highly coupled process that can affect the properties of the pre-detonation gas state.

Injection dynamics can also affect the mixing of reactants, which will vary the pre-gas state mixture composition ahead of the detonation wave. Sato et al. performed high-fidelity simulations of an RDC with an axial air inlet and found that the time-varying reinjection of reactants resulted in a stratified distribution of air and hydrogen [6]. The authors observed that the unbalanced fuel and air injector recovery alters the local mixture composition, promoting mixing with product gases and varying the detonation structure. The resulting computed peak pressure was significantly lower than in ideal detonation cases and matched experimentally measured values, but the predicted wave speed remained 20% higher than the measured one. The exact effect of the mixing is uncertain as the simulations showed regions of dilution of the fresh mixture by the remaining hot product gases, which can also weaken detonation properties. To isolate the impact of mixing on detonation properties, Gaillard et al. performed a three-dimensional numerical simulations of rotating detonation propagation on premixed and non-premixed injector configurations [9]. They observed that in the case of separate injection, the stratification of reactants results in a poor mixing efficiency, and as a consequence, less than 20% of reactants detonate. Both non-premixed and premixed configurations yield peak pressures at 20% of the CJ pressure. However, the detonation wave speed is 19% lower than the CJ one in the non-premixed configuration due to poor reactant mixing, and 5% lower in the premixed configuration due to hot gas effects on fresh reactants. The detonation process is therefore highly sensitive to transient mixing mechanisms, which create a stratified mixture.

The contact between fresh reactants and burned gases from the previous detonation cycle can also impact the detonation properties. Andrus et al. performed chemiluminescence experiments on an air-breathing premixed RDC and measured wave speeds lower than the CJ velocity [13]. They found that the partial mixing of reactants with detonation products resulted in an increase of temperature that can affect the propagation of the detonation wave. Fievisohn et al. also studied this phenomena through an idealized thermodynamic model assuming infinitely fast mixing to examine the effect of product recirculation [14]. Their analysis shows that the presence of product gases in the fresh reactant mixture can contribute to the velocity in the detonation, peak pressure, and wave speed. In their experimental study, Hansmetzger et al. arrived at a similar conclusion and suggested that the chamber geometry can modify the proportion of unburned gases, resulting in different wave speeds [15]. Product recirculation can also create favorable conditions for reactant deflagration before the arrival of the detonation wave. This mechanism is sometimes termed as parasitic combustion and has been observed in previous studies. In an OH* chemiluminescence imaging study, Chacon et Gamba observed autoignition kernels in the fill region, suggesting that the detonation propagates into an already deflagrating mixture [5]. Furthermore, a zero-dimensional model was constructed to study the effect of a partially vitiated mixture on detonation properties. Their measurements aligned with large computed values of vitiation volume fraction, on the order of 0.5, yielding a velocity and pressure ratio of 0.78 and 0.2 of the ideal CJ properties, respectively. Product recirculation can therefore impact the detonation propagation by modifying both the mixture composition and provoking partial pre-burning of the fresh reactants.

Product recirculation does not necessarily imply that parasitic combustion will occur, sufficient mixing is also a requirement and can affect the pre-detonation state. The theoretical studies mentioned above assumed perfect mixing between the products and the reactants, however Hansmetzger et. al compared their empirical results and thermo-chemical calculations and showed that non-adiabatic mixing of the reactants and products may need to be

accounted for to better predict the pre-detonation mixture [15]. Furthermore, Stechmann et al. studied the impact of product recirculation on autoignition time delays in rocket-type RDCs for different fuels [16]. Their reactor model shows that depending on the amount of mixing, the mixture may ignite on the time scales of the cycle time of the RDC. When the proportion of reactants to products reaches a certain level, their results show that the temperature is low enough the prevent ignition. In cases where parasitic deflagration occurs rapidly (relative to the detonation cycle time), a large portion of reactants may be consumed before the detonation arrives and the thermodynamic cycle will approach that of a constant-pressure burner. Fievisohn et al. also developed a reactor model to study the time-dependent mixing between products and reactants as an explanation for the reduced measured detonation velocity and peak pressures in premixed RDCs [7]. They show that if the mass fraction of products in the mixture reaches a certain threshold, deflagration will occur before the arrival of the detonation wave and result in weakened detonation properties. Their analysis identifies two modes of operation depending on whether the pre-detonation mixture autoignites. A strong mode characterized by speeds of approximately 85 to 100% CJ with no autoignition event and a marginal mode with speeds of approximately 60 to 70% CJ with autoignition event. Deflagration and mixing timescales should therefore be taken into account when determining the pre-detonation state.

Other mechanisms such as commensal combustion, wall heat transfer, viscous processes and lateral relief can also impact the propagation of the detonation wave inside the RDC. Recent studies suggest that there is a partial heat release through the detonation wave. In their OH* chemiluminescence experiments, Feleo et al. and Chacon and Gamba observed zones of chemiluminescence intensity in the post detonation products, suggesting that reactants combust after the passage of the detonation wave [5, 17]. This phenomenon, termed as commensal combustion, is the result of an incomplete reaction through the detonation wave, but the exact mechanism by which it occurs is not fully understood [18]. While not a direct measure of heat release, their resulting OH* chemiluminescence experiments showed that the fraction of heat release through the detonation could be estimated to be around 0.25-0.5 [18]. In addition to commensal combustion, it was also shown that wall heat transfers could result in a detonation velocity deficit. Strakey et al. computationally assessed loss mechanisms in an RDC environment and found that heat losses to the detonation walls are significant, while viscous losses at the wall are negligible [8]. Kaemming et al. assessed loss mechanisms through a reduced order thermodynamic model analysis and found that lateral relief, defined as the change of area through the detonation wave, could affect detonation properties [19]. The results of this study show that an increase in lateral relief in an RDE combustor produces detonation velocities less than the CJ velocities.

The mechanisms discussed above could reasonably contribute to the deficit of detonation properties observed in experiments. However, quantifying these processes using traditional RDC combustor diagnostics is difficult. The objective of this work is to develop a low-order model to identify the impact of non-ideal processes on these key detonation properties. Three mechanisms are studied: the buffer region created by non-premixed reactant injection, parasitic combustion of reactants, and suppression of the heat release through the detonation. A particularity of this model is that it is designed to utilize relatively easily measured experimental data as inputs. With this low-order model, key injection and combustion parameters that are not easily measurable in the RDC can be roughly estimated under more realistic conditions than those of idealized gas dynamics theory.

II. Methods

A. Experimental Setup

1. RDC Testing Facility

The data inputs for the models presented in this study were gathered on TU Berlin's modular rotating detonation combustor [20], shown in Figure 1. The combustor is composed of an annular chamber with an axial length L of 110 mm and an outer diameter D of 90 mm. The centerbody defines the annulus gap width Δ of 7.6 mm, yielding a combustor annulus area of 1967cm^2 . The TUB test facility is a non-premixed RDC that operates with hydrogen as fuel and air as oxidizer. The air is injected radially-inward through a thin slot, while the fuel is introduced axially in a jet in cross flow configuration. The fuel penetrates into the annulus through 100 evenly spaced injection holes with a diameter of 0.7 mm.

In the present study, a preliminary parametric analysis is performed to investigate the impact of air mass flow rates on the model. A single air injector configuration – a 1 mm gap height g – was considered. To impose back pressure on the combustion chamber, an outlet restrictions that reduced the outlet area by 25% was also introduced. The air mass flow rate was increased from 350 up to 550 gs^{-1} in increments of 25 gs^{-1}. The global equivalence ratio introduced into

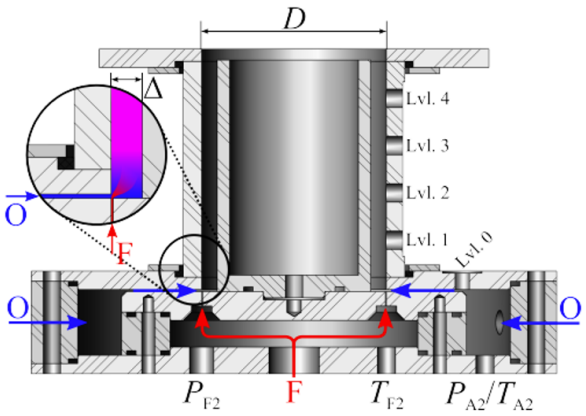

Fig. 1 Schematic representation of the RDC testing facility at TUB.

the annulus was set at stoichiometric conditions for all cases by changing the relative amount of reactant mass flow rates.

Both reactant flow rates are metered with sonic nozzles upstream of their respective plena, and are supplied at an ambient temperature of approximately 293 K. The reactant feed lines are pressurized prior to the experimental run to ensure that the desired mass flow rate is quickly reached. During testing, the reactant feed lines are controlled by dome-loaded pressure regulators with a time constant that is small compared to the reactant settling time. Settling times of 3 s for the air flow and 1 s for the fuel flow were set in order to achieve a steady flow prior to ignition. A spark plug, located in the region of the detonation front of the outer wall, serves to ignite the flow. During runs the combustion time is limited to 250 ms in order to limit the heat load on sensors and allow the combustion mode to stabilize inside the annulus.

2. Applied Instrumentation

Pressure diagnostics are placed in the reactant plena, and around the combustion chamber annulus. Oxidizer and fuel static plena pressures, p_{plA} and p_{plF}, were measured with flush-mounted Omega PXM319 transducers. The temperatures of the plena, T_{plA} and T_{plF} were measured with low-frequency thermocouples. As the present study focuses on the properties of the detonation zone, pressure diagnostics at the chamber wall were mounted on ports distributed circumferentially around that zone. A Kulite XTEL190 piezoresistive pressure transducer was installed in a recessed cavity in order to protect the sensor from the harsh conditions inside the annulus. The cavity-neck configuration of the recessed port was designed to resonate at a frequency of at least 80 kHz, far away from the 5-6 kHz frequency of the measured signal. To account for the cavity-induced attenuation of the signal, an in-house transfer function was used to map the attenuated signal measured by the recessed sensor to the "true" signal that would have been captured by a flush-mounted sensor during post-processing. An additional Kulite was placed in a capillary tube average pressure (CTAP) configuration with a tube standoff length of 1 m and inner diameter of 2 mm. The long thin line attenuates high-frequency components by viscous damping, thus providing a measurement of the mean absolute static pressure inside the annulus. The dynamic fluctuating pressure component at the chamber wall was measured using PCB 112A05 piezoelectric pressure transducers placed in a flush-mounted configuration. An additional recessed-cavity Kulite sensors was used as a reference against the measured data. Data acquisition was carried out with a sampling rate of 500 kHz. Signal amplifiers were constructed in-house for the Kulite sensors. PCB sensors were connected to PCB-specific charge converters and amplifiers.

3. Experimental Inputs to the Model

The dynamic inlet model and heat release models are based on experimental inputs measured in the TU Berlin RDC facility. There are three initial conditions for the dynamic inlet model: p_{pre} corresponds to the absolute static pressure before the arrival of the detonation wave and was measured by a recessed Kulite in the detonation zone. p_{avg} is a CTAP measurement corresponding to the mean absolute static pressure in the annulus. p_{plA} is the air static feed pressure obtained with a flush-mounted pressure transducer in the air plenum. It is assumed that the static pressure measured in the plenum, p_{plA} is equal to the stagnation pressure as the Mach number in the plenum is very low.

The heat release model is based on three inputs: the pressure just before the arrival of the detonation wave, p_{pre}, the average total temperature in the air plenum, T_{plA} and the global equivalence ratio, ϕ_g. p_{pre} is measured by flush-mounted Kulite measurements in the annulus. T_{plA} is measured by a low frequency thermocouple and is used to determine T_{avg} by isentropic expansion relations. Finally, the global equivalence ratio, ϕ_g is determined by the relative proportion of the total mass flow rates of reactants measured by sonic nozzles.

B. Low-Order Model

1. Overview of Model and Parameter Space

In the literature it was observed that wave speeds and peak pressure measured experimentally are often lower than those predicted by CJ theory and computed in CFD studies. The differences in detonation characteristics between experiments, numerical computations, and theory could stem from imperfect injection and mixing mechanisms, deflagrative burning, and partial detonation heat release. The objective of the present study is to provide insight into some of the governing processes inside an RDC using a low-order model of the pre-gas state. In the model, the effect of three mechanisms are considered: the formation of a buffer region (defined by psi), pre-deflagrative burning (defined by ω), and a partial heat release in the detonation zone (defined by χ). Each dimension represents the fuel (and subsequent heat release) that occurs or undergoes each of the processes as shown in Figure 2.

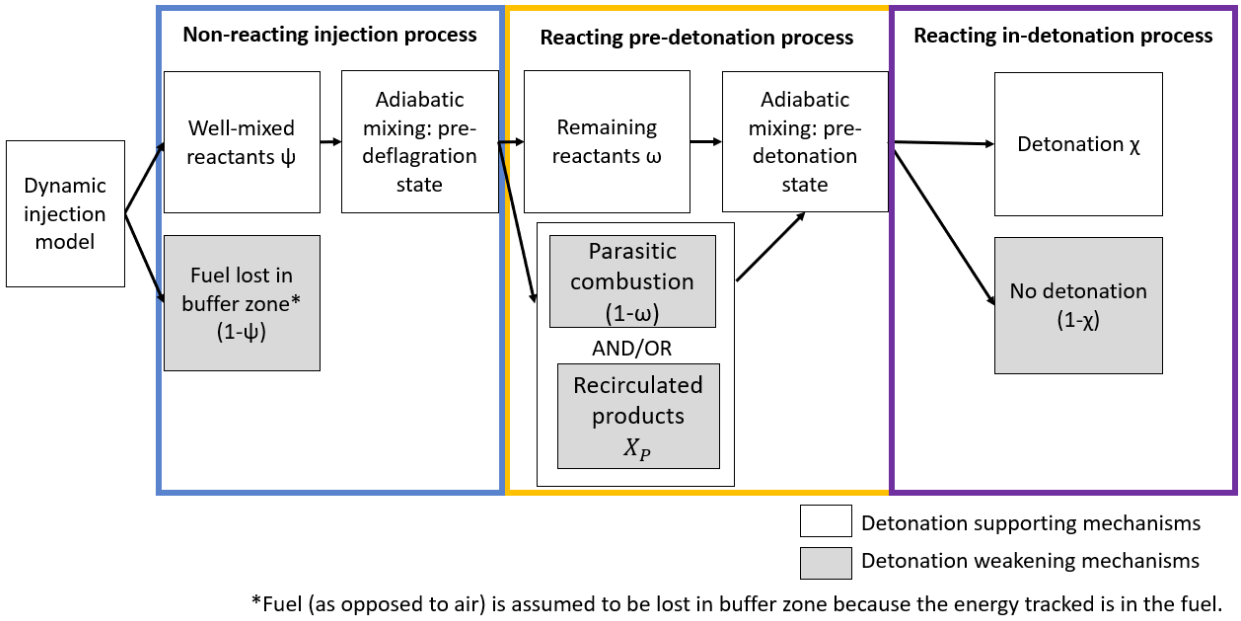

Fig. 2 Schematic representation of the low-order model constructed to assess the effect of three non-ideal processes: the buffer region, parasitic combustion, and detonation inefficiencies.

The low-order model is composed of a dynamic injection and heat release model. The steps of the low-order model can be summarized as follows: first, the dynamic injection model can determine the first parameter ψ, which accounts for the presence of the buffer region caused by disparate response times in non-premixed injectors. Here, ψ corresponds to the proportion of the fuel that is ultimately well-mixed, while the complement $(1-\psi)$ corresponds to the proportion of the fuel that is contained in the buffer zone. Typically, higher fuel plenum pressures indicate a faster reactant injector recovery time, and therefore this buffer region will correspond to a sequestration of fuel into a rich buffer zone. It is assumed that the portion of fuel outside of the buffer zone is then mixed adiabatically with air. The resulting mixture forms the pre-deflagration state.

A portion of the reactants are then assumed to deflagrate before the arrival of the detonation wave. The parameter ω is the proportion of the fuel that survives the injection and mixing period and will contribute to the heat release in the detonation. The complement, $(1-\omega)$ represents the heat release lost through parasitic combustion at constant pressure. As will be discussed, these two streams are adiabatically mixed and the resultant mixture is the defined reactant mixture

for the detonation. It should be noted that this approach is somewhat similar to the vitiation model by Chacon and Gamba [5], however in that work ζ represents the volume fraction of the mixture that goes through a deflagration. It should also be noted that ω does not distinguish between pre-deflagration and the recirculated products of the previous detonation. The net effect on the pre-detonation state will be very similar in terms of vitiation by combustion products. However, without distinguishing between these two processes, it is not possible to use such a low order model to determine combustion efficiency.

Lastly, χ represents the proportion of the heat release that occurs within the detonation and serves to drive the product gases to the sonic condition at the exit of the detonation. The complement $(1-\chi)$ then corresponds to the proportion of the fuel consumption or heat release that does not contribute to supporting the detonation wave (e.g. heat losses to the walls, non-uniform mixture, friction, etc.). At the moment, we do not explicitly state what the physical process(es) are that result in this detonation combustion inefficiency, but rather simply assume that these effects exist. The total fraction of heat release that supports the propagation of the detonation wave and that can contribute to pressure gain can be defined as $\nu = \psi\omega\chi$. For a CJ detonation, $(\psi, \omega, \chi) = (1, 1, 1)$.

2. Dynamic Inlet Model

A dynamic inlet model was developed to account for the impact of the temporal variation in reactant injection, namely the formation of the buffer layer and the variation of the local equivalence ratio on RDC operation. One objective of this model is to determine characteristic injector parameters such as the injector recovery times using commonly available experimental measurements. The algorithm of the model is summarized in Figure 3(a).

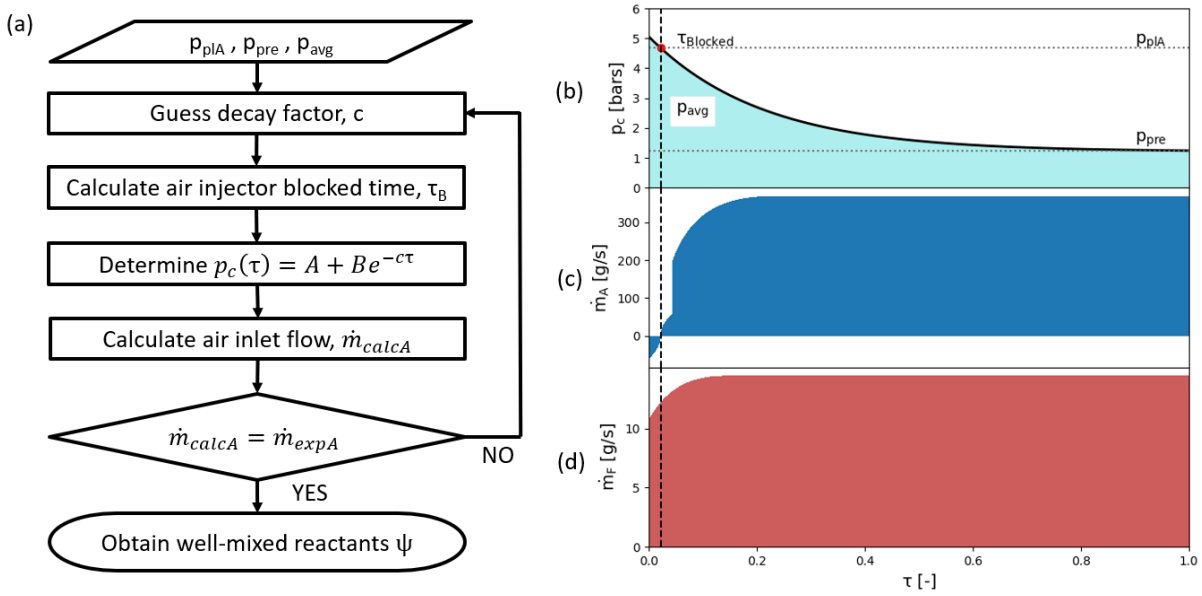

Fig. 3 (a) Outline of the dynamic injection algorithm, (b) Pressure decay function with the three pressure experimental inputs (c) Air mass injected and (d) Fuel mass injected over the non-dimensionalized wave period τ

It is assumed that the detonation wave in the annulus of the RDC can be modeled by a pressure decay function described in Equation (1), where A, B and c are scalar values. It can be noted that Equation (1) is similar to the general form of the pressure decay function used in previous studies as described in Equation (2) [19, 21, 22]. In these theoretical and numerical studies, the peak pressure, instead of the pre-detonation pressure, is used as a boundary condition to determine the pressure decay curve. At $\tau = 1$, Equation (3) approaches p_{pre} only for steep-fronted waves with large values of c. In the case of more gradual waves, Equation (3) does not necessarily converge to p_{pre}. In this experimentally-based model, the peak pressure is generally very difficult to capture accurately and is quite dependent on the sensor installation and data acquisition and filtering processes. It is more likely that the sensor is better able to capture the pressure to which the gases expand, namely the pre-detonation pressure. Since the pre-detonation pressure is chosen as a boundary condition, the form presented in Equation (1) was used.

$$p_c(\tau) = A + Be^{-c\tau} \quad \text{with} \quad \begin{cases} p_c(\tau_B) = A + Be^{-c\tau_B} = p_{plA} \\ p_c(1) = A + Be^{-c} = p_{\text{pre}} \\ \int_0^1 p_c(\tau)d\tau = A + \frac{B}{c}\left(1 - e^{-c}\right) = p_{\text{avg}} \end{cases} \tag{1}$$

$$p'_{\text{decay}}(\tau) = p_{\text{pre}}\left[1 + \left(\frac{p_{\text{peak}}}{p_{\text{pre}}} - 1\right)e^{-c\tau}\right] \tag{2}$$

$$p'_{\text{decay}}(1) = p_{\text{pre}}\left[1 + \left(\frac{p_{\text{peak}}}{p_{\text{pre}}} - 1\right)e^{-c}\right] \approx p_{\text{pre}} \qquad \text{for } c \gg 1 \tag{3}$$

The model is based on an initial guess of the exponential decay factor, c, from which a pressure decay function is determined as shown in Figure 3(b). The function is defined on a wave-period normalized axis τ. It is noted that p_{peak} does not represent the pressure at the von Neumann state behind the leading shock front, but the pressure reached at the sonic plane (assuming that the detonation wave can be considered to be thin). To determine the decay rate of the pressure decay function, three boundary conditions are used: p_{pre}, p_{avg} and p_{plA}. p_{pre} corresponds to the pressure before the arrival of the detonation and is therefore, by the nature of the detonation cycle, assumed to be the pressure of the expanded product gases at $\tau = 1$. p_{avg} corresponds to the mean value of the pressure decay function over the wave period and p_{plA} to the air plenum pressure. Since in-annulus pressures greater than or equal to the plenum pressure represent cases where forward flow is blocked, the time at which $p(\tau) = p_{\text{plA}}$ is denoted τ_B and represents the fraction of time during which flow is blocked over a wave period. The non-dimensional blocked time of the air injector, τ_B, is directly determined from the value of the decay factor, c, for each iteration as shown in Equation (4).

$$\tau_B = -\frac{ln\left(\frac{p_B - p_{\text{pre}}}{p_{\text{avg}} - p_{\text{pre}}}\left(-\frac{1}{c}e^{-c} + \frac{1}{c} - e^{-c}\right) + e^{-c}\right)}{c} \tag{4}$$

Once the non-dimensional air injector blockage time, τ_B, has been calculated, the pressure decay function can be determined. The instantaneous mass flow rates across the air injector can then be calculated from the pressure ratio between the air plenum and annulus as shown in Figure 3(b). The instantaneous choked and unchoked mass flow rates for a one-dimensional isentropic and compressible flow through an area, A, are given respectively in Equations (5) and (6) [23]. The subscripts $_{\text{up}}$ and $_{\text{down}}$ denote the upstream and downstream pressures that can be modified accordingly to the direction of the flow. There are six possible flow cases that can occur: reverse choked and unchoked product flow, forward choked and unchoked product flow and forward choked and unchoked reactant flow. If flow reversal of products into the plenum occurs, then the products must be injected back into annulus before reactants can enter. This point, known as the injector recovery time, τ_{r}, is found by accounting for the total reverse mass of products into the plenum. It is assumed that the reactants and products do not mix inside the plenum. The temperature of the reactants is therefore fixed by the temperature measured in the plenum, and the temperature of the product is calculated by prescribing a peak static detonation temperature and assuming isentropic expansion of products behind the wave. The sudden change in gas composition results in a discontinuity in the mass flow rates at τ_{r}. In a physical case mixing is expected to occur between the products and reactants, however this is beyond the scope of the present low-order model.

$$\dot{m}(\tau) = \frac{p_{\text{up}}A}{\sqrt{R_{\text{up}}T_{\text{up}}}}\sqrt{\gamma\left(\frac{2}{\gamma_{\text{up}}+1}\right)^{(\gamma_{\text{up}}+1)/(\gamma_{\text{up}}-1)}} \tag{5}$$

$$\dot{m}(\tau) = \frac{p_{\text{up}}A}{\sqrt{R_{\text{up}}T_{\text{up}}}}\sqrt{2\frac{\gamma_{\text{up}}}{\gamma_{\text{up}}-1}\frac{p_{\text{up}}}{p_{\text{down}}}^{\frac{2}{\gamma_{\text{up}}}}\left[1 - \left(\frac{p_{\text{up}}}{p_{\text{down}}}\right)^{\frac{\gamma_{\text{up}}-1}{\gamma_{\text{up}}}}\right]} \tag{6}$$

Once the instantaneous mass flow rates are found, they are summed to find the total injected mass of air over one wave period. The computed value is compared to the experimental one metered by the sonic nozzle. The value of the decay factor, c, is iterated until mass convergence of air is reached within a ±5% tolerance. The obtained pressure decay curve is then applied to the fuel injector. The resulting instantaneous fuel mass flow injected over one wave period is displayed in Figure 3(d). The calculated air and fuel mass can then used to determine parameters such as the fraction of well-mixed reactants, ψ, and the deflagration equivalence ratio, ϕ_{def}, as will be detailed in the next subsection.

It can also be noted that in studies from Kaemming et al. and Shepherd and Kashara, the decay rate, c, is empirically determined by fitting Equation (2) to CFD data [19, 21]. In the present model, the decay rate is determined through an iterative procedure with the average, plenum and pre-detonation pressures as inputs. This approach is similar to the model presented by Bedick et al. [22], where the decay factor can be determined using an iterative solver to match the average pressure given a peak and pre-detonation pressure. However, in Bedick's low-order model, once the decay factor was found, the pressure decay function was set and the plenum pressure was iterated. In the present study, the plenum pressure is an input measured experimentally, and the scaling factor is changed to yield different pressure decay shapes until mass convergence is met.

3. Heat Release Model

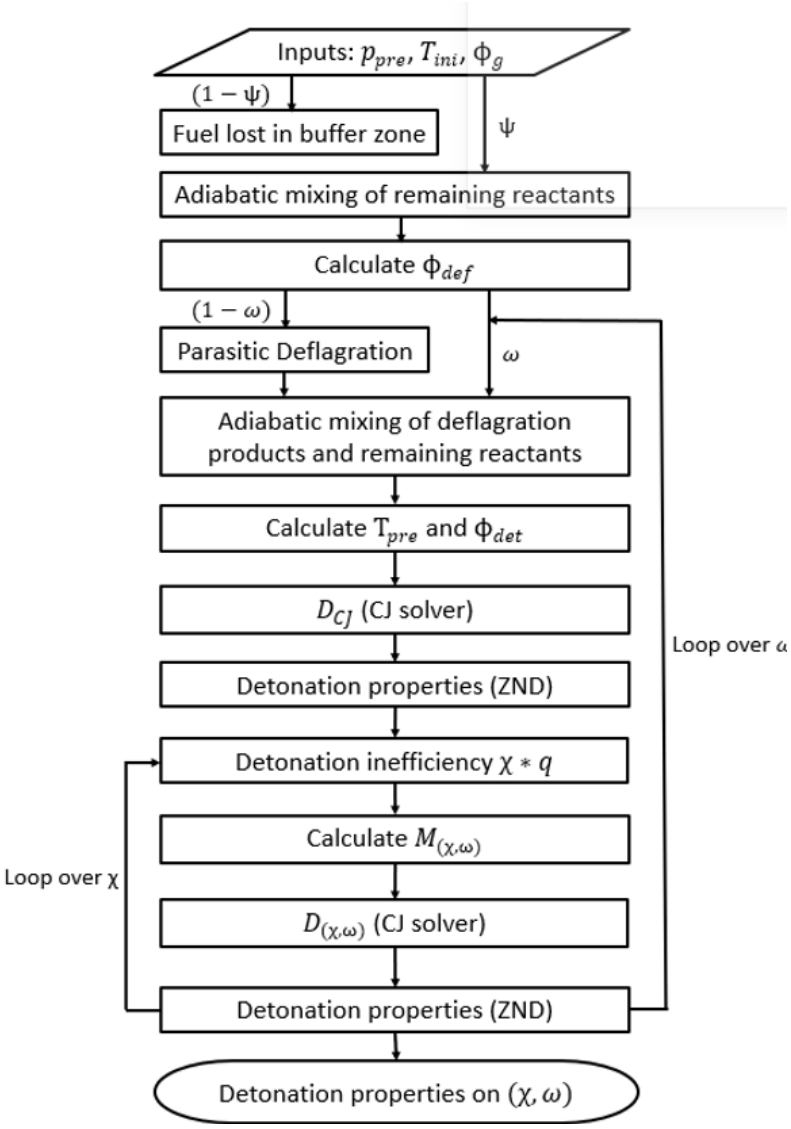

Fig. 4 Outline of the heat release algorithm

The algorithm of the heat release model is summarized in Figure 4. Chemistry calculations are carried out using Cantera [24]. All results are computed with the mechanism of San Diego [25] using H_2 and simplified air. CJ and ZND calculations for a one-dimensional ideal steady compressible flow are then performed using the Shock and Detonation toolbox for Cantera [26]. There are three inputs to the heat release model: the pressure just before the arrival of the

detonation wave, p_{pre}, the average temperature in the annulus, T_{avg}, and the global equivalence ratio, ϕ_g. The steps of the heat release model can be summarized as follows: First, the fuel sequestered in the buffer region must be accounted for. The buffer region is dependent on the imbalance in injector response times. Assuming that the fuel injector has a faster response time, the buffer region has an equivalence ratio higher than the "global" one. If a portion of the global fuel injection is sequestered in the buffer region, the equivalence ratio of the well-mixed zone must be less than ϕ_{g}. If ψ represents the mass fraction of well-mixed fuel, it can be determined from the ratio of the integrated mass flow into the annulus starting at the recovery time of the air, τ_{RA}, and at the recovery of the fuel, τ_{Rf} as shown below in Equation (7). τ_{RA} and τ_{Rf} are both outputs of the dynamic inlet model. It is assumed that the static pressure measured in the plenum, $\overline{p}_{\text{plA}}$ is equal to the stagnation pressure as the Mach number in the plenum is very low.

$$\psi = \frac{\int_{\tau_{RA}}^{1} \dot{m}_f d\tau}{\int_{\tau_{Rf}}^{1} \dot{m}_f d\tau} \tag{7}$$

The effective, local equivalence ratio, ϕ_{mixed} for the parasitic combustion can therefore be calculated from ψ as shown in Equation (8).

$$\phi_{\text{def}} = \frac{\text{OF}_{st}}{\text{OF}} = \frac{\phi_g \text{OF}_g}{\text{OF}} = \phi_g \frac{\int_{\tau_{RA}}^{1} \dot{m}_f d\tau}{\int_{\tau_{Rf}}^{1} \dot{m}_f d\tau} = \phi_g \psi \tag{8}$$

The remaining reactants are then assumed to be mixed infinitely fast. Then, a proportion of the reactants $(1-\omega)$ undergoes a constant pressure combustion process to chemical equilibrium. The portion of deflagrated products is then adiabatically mixed with the remaining reactants, ψ, and the adiabatic temperature of the mixture is calculated using Equation (9). The resulting mixture of reactants and products is held frozen until the detonation wave arrives.

$$T_{\text{def}} = \frac{C_{\text{p,prods}} * T_{\text{prods}} + C_{\text{p,reacts}} * T_{\text{avg}}}{C_{\text{p,prods}} + C_{\text{p,reacts}}} \tag{9}$$

The local equivalence ratio for the detonation process is then calculated. This parameter is impacted by both ω and, implicitly, ψ. If the initial mixture is globally lean, a portion of the air that goes through the deflagration and that remains in the products mixes with the remaining surviving reactants. The resulting mixture for the detonation is then diluted by this surviving oxidizer, shifting the local mixture further lean. This effect is more pronounced the further the global equivalence ratio is from stoichiometric as shown in Figure 5(a). Therefore, if ϕ_{mixed} is lean, ϕ_{det} is leaner if more of the initial mixture goes through parasitic combustion (i.e. decreasing values of ω). In the case of a stoichiometric mixture, the equivalence ratio remains unchanged for the detonation.

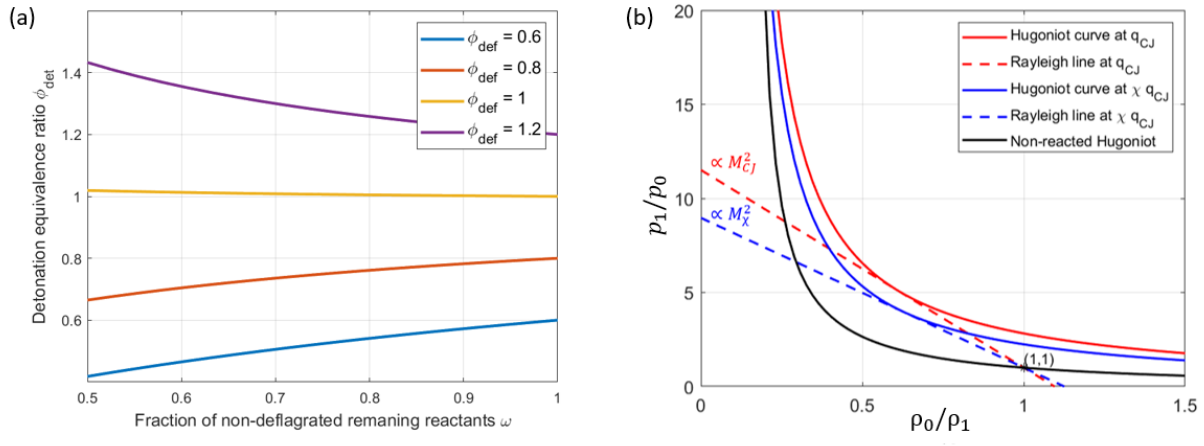

Fig. 5 (a) Variation of the detonation equivalence ratio, ϕ_{det} versus the fraction of remaining reactants, ω, (b) Rayleigh-Hugoniot (RH) curves calculated from the heat-release model. The blue and red RH curves are respectively obtained for an ideal heat release process (χ = 1) and non-ideal heat release process (χ < 1). The slope of the Rayleigh lines are proportional to the square of the detonation Mach number,

Once the pre-detonation mixture composition and state have been determined, the detonation velocity is then obtained from the SDT CJ solver. Detonation properties at the CJ point are calculated using the ZND solver for a one-dimensional ideal steady compressible flow. From ZND theory, the maximum heat release that occurs within the detonation and that drives the product gases to the sonic condition, q_{CJ}, can be calculated for a given initial CJ Mach number according to Equation (10). It is assumed that the mixture is a perfect gas with a constant heat capacity ratio, γ. Although γ varies from the initial to the final state, this does not significantly alter the resulting heat release value.

$$2\left(\gamma^2-1\right)\frac{q_{CJ}}{c_0^2}=\frac{\left(M_{CJ}^2-1\right)^2}{M_{CJ}^2\left(1+\frac{\gamma-1}{2}M_{CJ}^2\right)} \tag{10}$$

In Figure 5(b), the square of the initial Mach number, M_{CJ} determines the slope of the Rayleigh line, and q_{CJ} determines the equilibrium Hugoniot. The parameter χ is then used to scale q_{CJ} such that χq_{CJ} represents the modified heat release needed to choke the product gases. The partial heat release reduces the slope of the Rayleigh line. As expected, the resulting Hugoniot curve lays between the non-reacted and fully-reacted Hugoniot defined as $\chi = 1$. The reduced Mach number, M_χ, is then obtained from a modified version of Equation (11).

$$2\left(\gamma^2-1\right)\frac{\chi q_{CJ}}{c_0^2}=\frac{\left(M_\chi^2-1\right)^2}{M_\chi^2\left(1+\frac{\gamma-1}{2}M_\chi^2\right)} \tag{11}$$

From this approach, the resultant detonation Mach number M_χ accounting for the reduced contribution of heat release in the detonation wave, the impact of the pre-combustion on the initial mixture state, and the shift in the local equivalence ratio due to the formation of a buffer region can be accounted for. The reduced wave speed and detonation properties are then obtained as before from the CJ and ZND solvers respectively. By iterating over several values of ω and χ, the detonation properties can be obtained for different pre-gas states and detonation heat release. Given a set of boundary conditions, the resulting detonation wave speeds and peak pressures over the (χ, ω) domain are plotted in Figure 6. The filled contours and black line contours show respectively the variation of the calculated detonation wave speeds and peak CJ pressures with ω and χ. The parameters are normalized by the CJ values for a perfect detonation, specifically for $\psi = \omega = \chi = 1$. For increasing values of χ and ω, the normalized wave speed and peak pressure increase, approaching a perfect detonation in the upper right-hand corner of the domain at $(\chi = 1, \omega = 1)$. At certain values of χ and ω, particularly in the upper left-hand corner, the mixture fails to detonate and no detonation parameters are plotted.

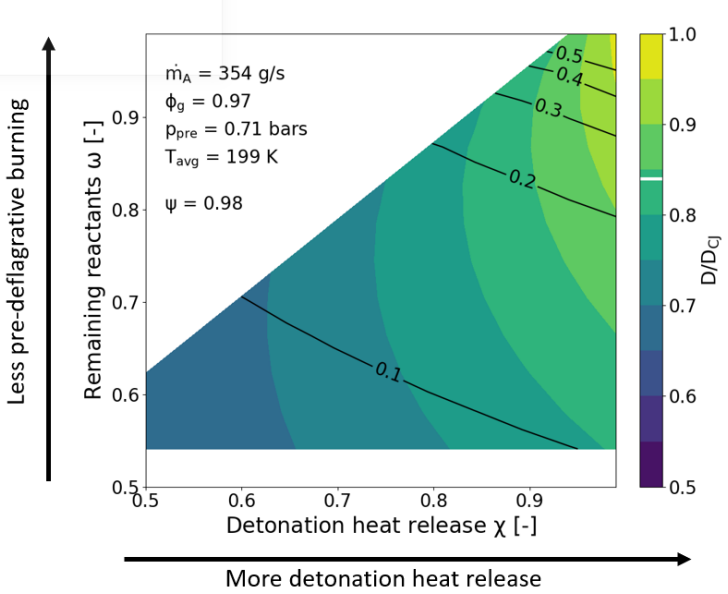

Fig. 6 Variation of the detonation wave speed (filled colored contours) and peak pressure (black contour lines) on the (χ, ω) domain.

III. Results

The overarching objective of this work is to estimate, using a low-order model, non-ideal processes and their effect on detonation properties. A parametric analysis is carried out to provide an initial validation of the low-order model and assess the impact of boundary conditions on the key model outputs. In this preliminary parametric study, eight test cases of varying air mass flow rates are considered. The RDC is operated at a stoichiometric equivalence ratio and the mass flow rates are increased from 350 g/s to 550 g/s. With this combustor configuration and operating conditions, detonation modes considered are limited to single detonation wave cases.

A. Dynamic Injection Model

1. Model Validation and Sensitivity Analysis

The dynamic injection model and its resulting key injection properties, specifically the injector response times and the parameter ψ, were first considered. To assess the validity of the dynamic injection model, the pressure decay curve and calculated mass flow rates obtained from the dynamic injection model were compared to measurable experimental data. It is noted that the pre-detonation pressure is here defined as the pressure at $\tau = 0.9$ due to the undershoot caused by the application of the transfer function on the Kulite pressure measurements at $\tau = 1$. Figure 7(a) displays the computed pressure curve and pressure traces measured by the piezoresistive Kulite sensor (with the transfer function correction applied) for an air mass flow rate of $\dot{m}_A = 354$ g/s. It can be observed that the calculated peak pressure at $\tau = 0$ is greater than the maximum measured pressures by an average of 2 bar. The difference between measured and modeled peak pressures is expected due to the finite response time of the pressure sensor which is unlikely to accurately capture the highest peak pressures. Therefore, the peak pressures measured by the sensor do not correspond to the CJ state, but to a later state where product gas expansion has already started. As the product gas expansion is most likely better captured by the Kulite, the pressures for $\tau \geq 0.15$ are compared to the modeled decay rate. It can be observed that the modeled function falls below the measured Kulite traces for $\tau \leq 0.4$, indicating that the computed curve has a higher decays rate than the measured signal. Similar trends were observed for the other mass flow rates. This over-expansion can be partly attributed to the air mass flow convergence, which drives the pressure curve down. In addition, as will be shown subsequently uncertainties in the pressure inputs can affect the shape of the predicted curve. Overall, the dynamic injection model does not capture the experimental decay rate for lower values. To give a more representative depiction of the detonation wave and product gas expansion, alternative boundary conditions could be chosen. This will be discussed in a future study.

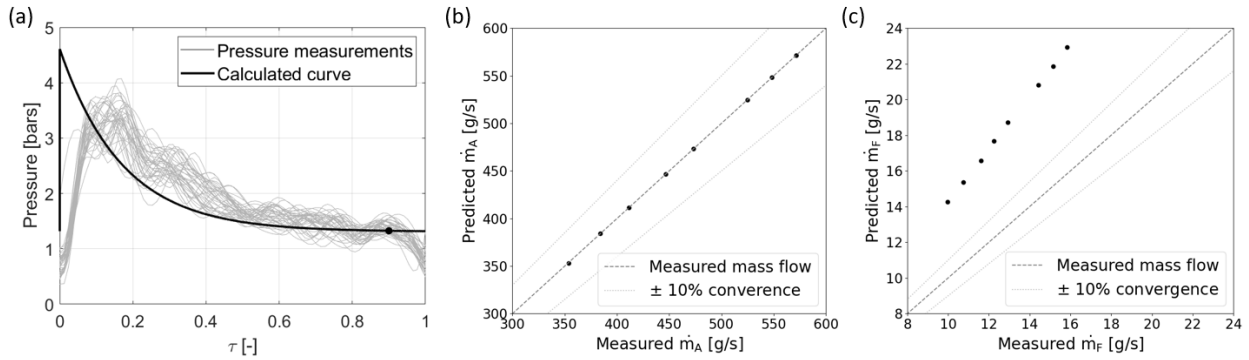

Fig. 7 (a) Comparison of measured Kulite traces (after post-processing via the transfer function) and predicted pressure decay curve for the measured air mass flow rate of $\dot{m}$ = 354 g/s and (b) Comparison of the measured and predicted air mass flow rates and (c) Comparison of the measured and predicted fuel mass flow rates

Model validation was also checked by comparing the calculated mass flow rates were compared to measurable experimental data. As the dynamic injection model is based on the mass continuity of the air injector, good agreement between the experimental and calculated air mass flow rates can be expected as shown by 7(b). While the air mass flow rates are well-captured by the model, the fuel mass flow rates are considerably over-predicted by the model as shown by Figure 7(c). The lack of convergence between the experimental and modeled data is due to the fact that the dynamic injection is predicated solely on mass continuity across the air injector. This assumption was deemed suitable as the

proportion of fuel only amounts to 2% of the total reactant mass. To meet the air mass flow convergence criteria set mainly by the air plenum pressure, the model under-predicts the pressure decay curve. Since the measured pressure in the fuel plenum is much higher than in the air plenum as displayed in 9(a), this leads to an over-prediction of the fuel mass flow. Another possible explanation that is currently being investigated is the potential formation of a vena contracta boundary layer in the fuel injector after ignition, which would result in a reduced fuel injector effective throat area. Overall, the comparison between the modeled and experimental reactant flow rates, shows that the low-order model predicts accurately the air mass flow and significantly over-predicts the fuel mass flow. To improve convergence of the computed mass flow rates with the measured ones, improved modeling of the injector areas, gas temperatures and gas properties will be implemented in a future work.

As the dynamic injection model is based on a guess of the decay factor from which the last boundary condition needed to close the pressure decay equation can be determined, the sensitivity of the outputs to the decay factor was also studied. Figure 8(a) shows the variation of the air mass flow and the blocked time with different values of the decay factor for a measured air mass flow of $\dot{m}_A = 354$ g/s. It can be observed that for $c < 15$, increasing the decay factor, leads to a rapid increase in the blocked air injector time, while for $c > 15$, increasing the decay factor causes a slow decrease of the blocked air injector time. For a measured $\dot{m}_A = 354$ g/s the closest air mass flow is reached at $c = 6$, thereby yielding a moderate decay curve. In all cases considered, the model returns a pressure decay function with a moderately value of c, where the dynamic model is very sensitive to c.

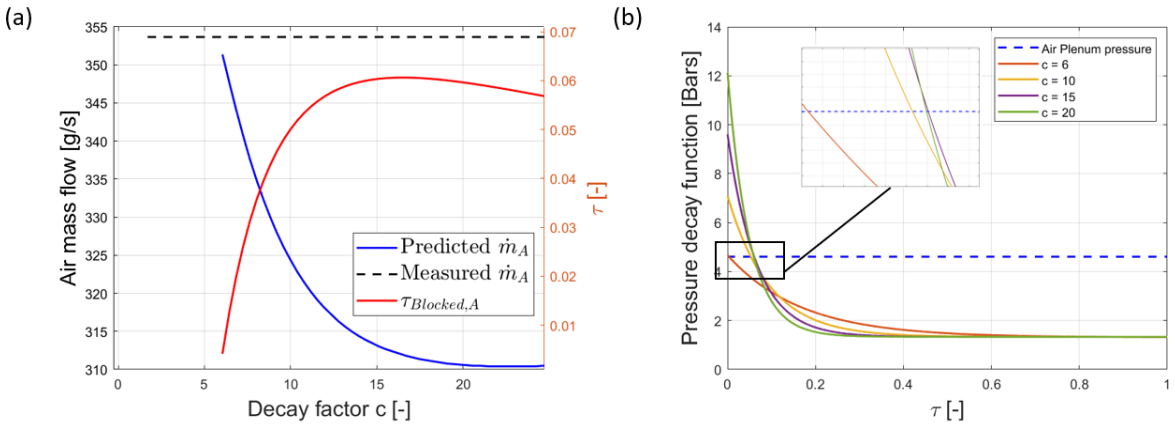

Fig. 8 (a) Variation of the calculated air mass flow (blue curve) and blocked air time (red curve) with the decay factor (b) Pressure decay curve versus normalized time for different decay factors. Both plots are obtained for a measured air mass flow rate of $\dot{m}_A = 354$ g/s

2. Parametric Analysis

The parametric study was performed on the dynamic injection model to determine the effect of mass flow variation on key injection properties, specifically, the injector response times and the parameter, ψ. The variation of the experimental inputs, namely, p_{pre}, p_{avg} and p_{plA} the dynamic model are first investigated as shown on Figure 9(a). As expected, the three pressure input boundary conditions follow overall a linearly increase with mass flow rate. The computed pressure decay curves are plotted on Figure 9(b). From Figure 9(b), it can be observed that the maximum pressure at $\tau = 0$ increases with the mass flow rate, indicating that a higher pressure is reached across the detonation wave with increasing air flow rates. In addition, as displayed on Figure 9(c), the decay factor, c, increases with mass flow rate resulting in a steeper curve. The increase in the detonation strength with increasing mass flow rates is expected. The obtained normalized blocked and recovery times of the air injector are plotted on Figure 9(d). For the air injector, the blocked and recovery times increase with mass flow rate, reaching a maximum of 2% and 4%, respectively, at $\dot{m} = 565$ g/s. The air injector recovery time is smaller by roughly a factor of two than values obtained in previous experimental and numerical studies [4, 5, 13, 27]. The fuel blocked and recovery times (not plotted here) are zero for all cases due to the fact that fuel plenum pressure is higher than the maximum pressure calculated as shown on Figure 9(a). The under-prediction of the blocked and recovery time of the air injector times results in values of ψ close to 1, implying that the portion of fuel sequestered in the buffer zone is less than 2% across the mass flows considered From Figure 9(c).

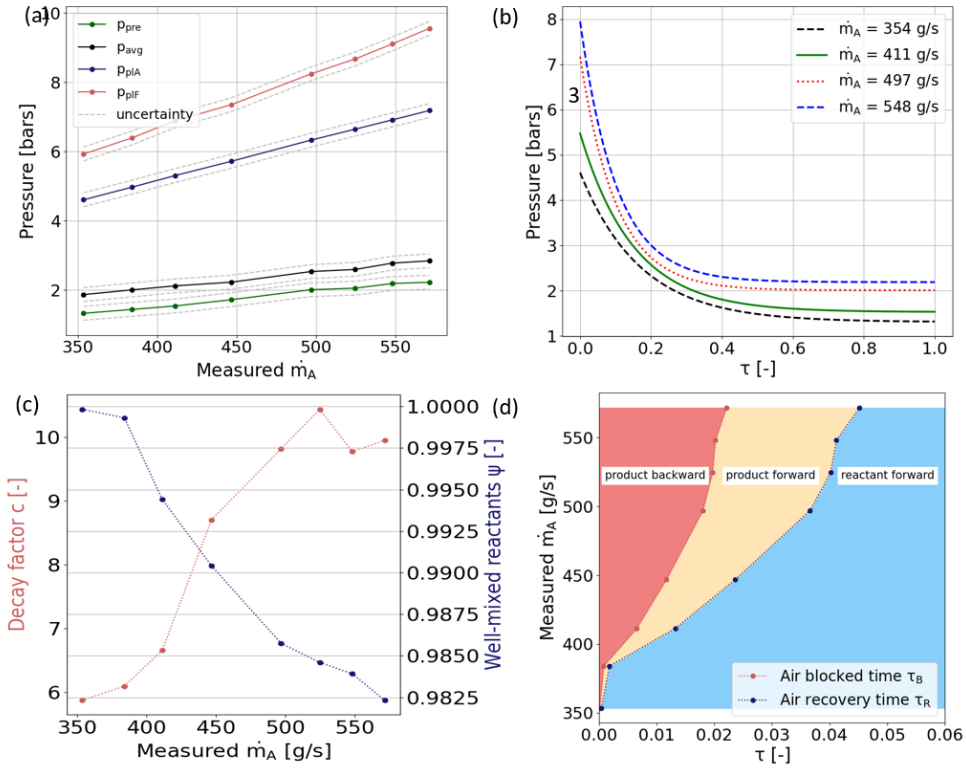

Fig. 9 (a) Variation of the pre-detonation, average, air plenum and fuel plenum pressures with the measured air mass flow, (b) Computed pressure decay curves for four mass flow rates cases, (c) Variation of the decay factor, c and the proportion of the fuel that is well-mixed, ψ with the measured air mass flow, (d) Variation of the blocked and recovery injector time with mass flow rates.

B. Heat Release Model

1. Model Sensitivity

The outputs of the dynamic injection model, as discussed in the previous section, determined the post-injection state for each air mass flow case. From these results, the parametric study was then performed on the heat release model to determine the effect of mass flow variation on the reacting pre-detonation and in-detonation processes, ω and χ. A sensitivity study was performed to evaluate the impact of the three experimental input parameters, the initial temperature, pre-detonation pressure and global equivalence ratio on the detonation wave speed, pressure ratio and pressure peak as shown in Figure 10. The results give insight on which parameters can be used to find the convergence between experimental and computed values on the (χ, ω) domain. For instance, as shown in Figure 10(f), the peak pressure is very sensitive to the inlet pressure, thus uncertainties in inlet pressure measurements could significantly affect the convergence between calculated and measured peak pressure values. In this case, given an empirical inlet pressure, the pressure ratio is a more robust measure of convergence. Furthermore, the results of the sensitivity analysis also highlight where additional experimental and numerical data is needed to define more realistic inlet boundary conditions. As shown in Figure 10(d), the wave speed is particularly sensitive to the global equivalence ratio. Numerical studies of the TUB RDC configuration have reported that the reactant mixture inside the annulus is stratified with portions of lean and rich reactants fraction [4]. To account for variations in the mixture composition, future versions of the model will integrate a distribution function for the global equivalence ratio.

The sensitivity of the detonation properties to the mechanisms ψ, ω and χ was then assessed. Figures 11(a-c) show the variation of the modeled wave speed and peak pressure for different values of ψ, ω and χ respectively. From Figure 11(a), it can be observed that increasing values of ψ yield a linear increase in detonation wave speed and peak pressures. As shown by Figure 11(b), the pressure peak follows an exponential growth as ω approaches one. This variation is expected and follows same trends as previous numerical and low-order recirculation models [10, 14, 15].

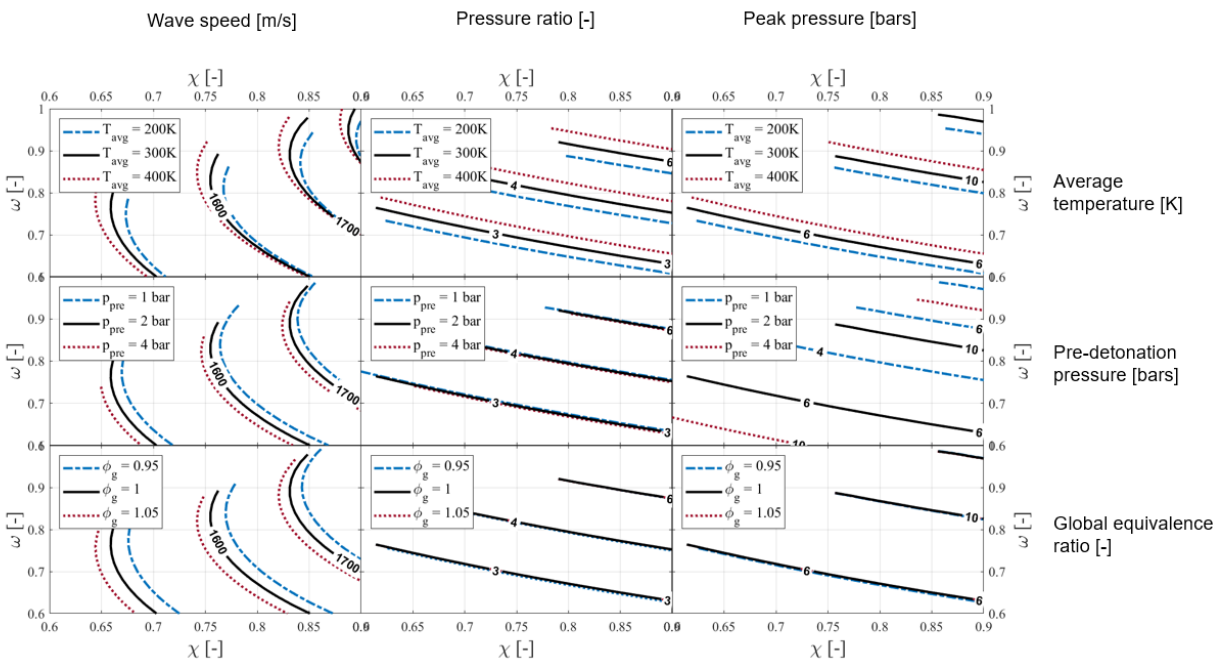

Fig. 10 Sensitivity study of experimental inputs on the heat release model outputs. The top, middle and bottom rows represent the effect of the variation of the average temperature, pre-detonation pressure and global equivalence ratio respectively. The left, middle and right columns depict the variation of the wave speed, pressure ratio and pressure peak respectively. The base standard case is defined at T_{avg} = 300 K, p_{pre} = 2 bar and ϕ_g = 1.

From Figure 11(c), it can also be observed that the detonation properties vary linearly with χ.

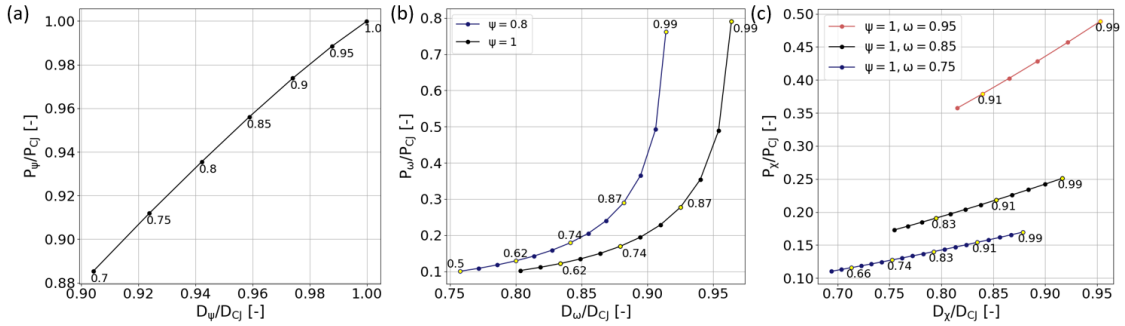

Fig. 11 Variation of wave speed and peak pressure (normalized by CJ values) (a) for different values of ψ, (b) for different values of ω (c) for different values of χ.

2. Parametric Analysis

A parametric study was performed on the heat release model to determine the effect of mass flow variation on the reacting pre-detonation and in-detonation processes, ω and χ. For each mass flow rate case, the wave speed and peak pressures were calculated for different combinations of (χ, ω) and then compared to the peak pressure, pressure ratio (computed from the dynamic model) and the experimental wave velocity as displayed on Figure 12. If the measured wave speed, peak pressure and pressure ratio intersect in the (χ, ω) domain, then the parameters ω and χ can be estimated for a given experimental case. This approach found good agreement for the four smallest mass flows. The resulting modeled (χ, ω) domain and measured wave speed and calculated peak pressure are presented Figure 12. It can be noted that the normalized pressure ratio has here not been plotted as its contour matches exactly with the normalized

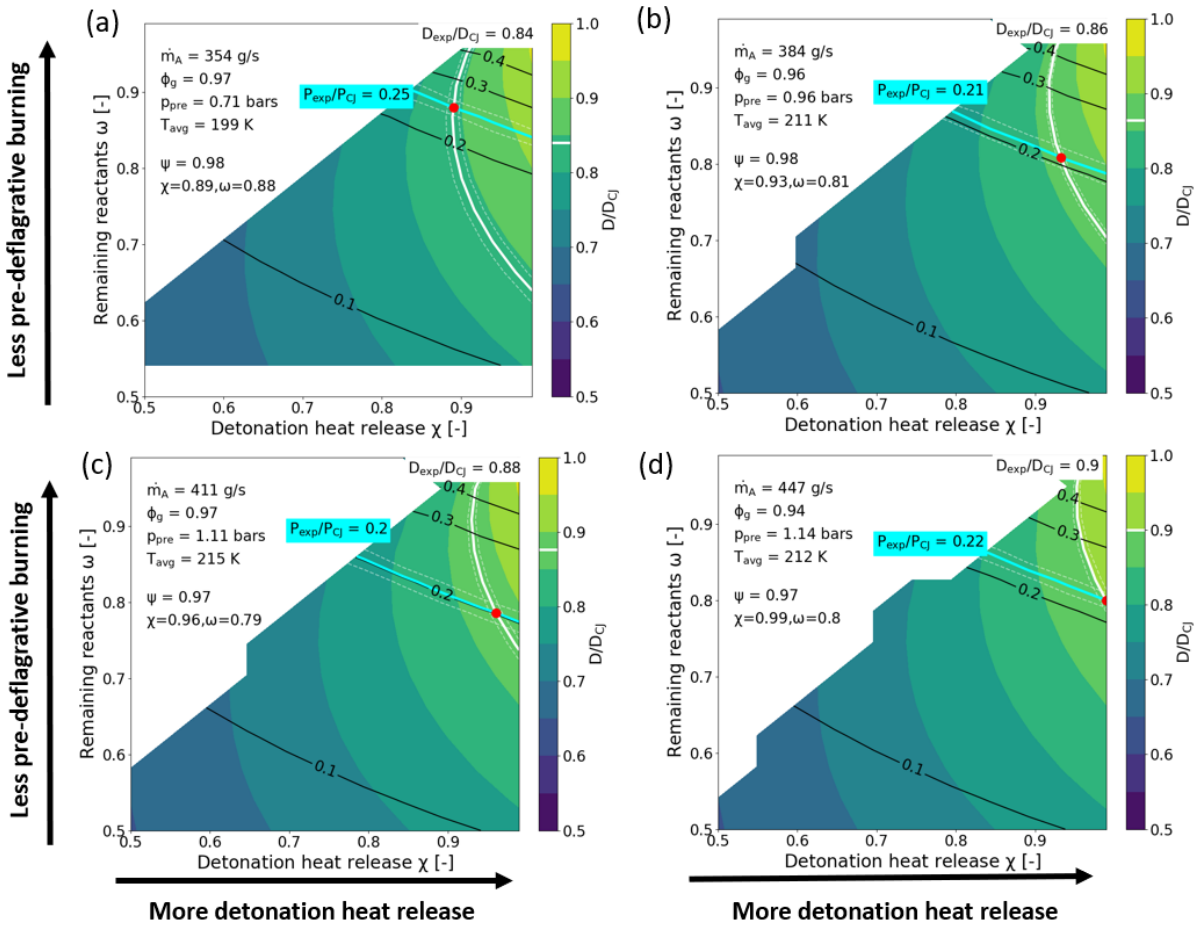

Fig. 12 Solution domain converged mass

peak pressure. In general, the experimental wave speed and modeled peak pressure intersect in the upper right-hand corner of the domain, at relatively high values of χ's and ω's. For example, from Figure 12(a), at $\dot{m} = 354$ g/s, the measured wave speed and calculated peak pressure at $(\chi = 0.89, \omega = 0.88)$. The value $\omega = 0.88$ can be interpreted as follows: out of the well-mixed fuel from the injection, 88% can potentially contribute to the detonation heat release, 12% pre-deflagrates. Similarly, $\chi = 0.89$ means that out of the fuel that survived injection and pre-deflagraton, 89% support the detonation heat release and 11% do not. As the mass flow increases, the intersection point moves towards increasing values of χ's and decreasing values of ω's. The shift of the intersection point is caused by the increase of the measured wave speed and decrease of the calculated peak pressure with mass flow rates. Figure 12(d) shows that for $\dot{m} = 447$ g/s, the curves intersect at $(\chi = 0.99, \omega = 0.8)$, indicating that out the well-mixed reactants 80% of fuel survives the pre-deflagration process and of that, 99% will detonate.

From Figure 2, it can be seen that there are four outcomes for the initial fuel packets: (1) they are sequestered in the buffer zone $(1-\psi)$, (2) they undergo $(1-\psi)*(1-\omega)$, (3) they survive the pre-deflagration but do not contribute to the heat release in the detonation $(1-\psi)*(1-\omega)*(1-\chi)$ or (4) they support the detonation the detonation $(\psi*\omega*\chi)$. The resulting proportion of fuel for each outcome for the four converged mass flow rates is plotted in Figure 13. It can be observed that the energy sequestered into the buffer zone is relatively constant across all mass flow rates and varies between 3% to 6%. This is reasonable considering the constant injector design and equivalence ratio. The proportion of heat lost during the pre-deflagration increases from 16% to 20% from 350 g/s to 450 g/s. The proportion of remaining energy not contributing to the detonation decreases from 6% to 1% with increasing mass flow rates. The simultaneous increase in pre-deflagration and decrease in non-detonated reactants offset each other, and result in an overall constant in-detonation heat release $(\psi*\omega*\chi)$ over the mass flow rates considered.

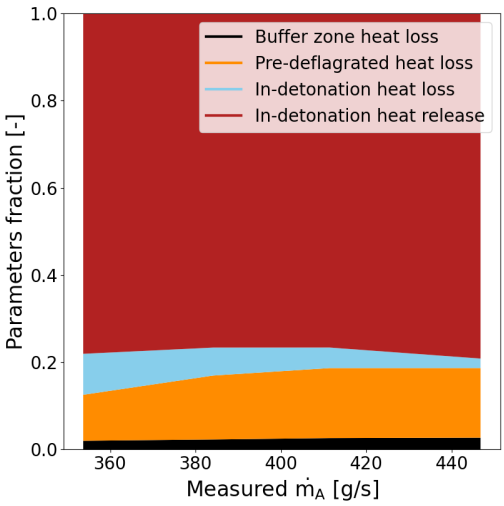

Fig. 13 Fraction of heat release, fate of fuel pocket, maybe should plot the y-axis in percents, might be easier to understand

3. Non-converged Cases

For the remaining mass flow cases, the measured wave speed and calculated pressure peak do not intersect in the domain for the given conditions shown in Figure 14(a). The lack of convergence occurs because the wave detonation velocity increases, while the calculated peak pressure decreases as shown from Figure 14(b). It is probable that the dynamic injection model struggles to capture the peak pressure of the detonation wave, particularly at higher mass flow rates where the detonation wave is stronger. As the peak pressure gets higher (as happens with the high mass flow cases), the model becomes more sensitive as the the peak pressure follows an exponential-like growth when ω approaches one. Since it is difficult to capture experimentally high pressures, it becomes increasingly difficult to move toward the top right-hand corner of the domain and and therefore reach convergence. The lack of convergence is thus due to the difficulty in capturing the experimental initial conditions, rather than an error in the model. Improving the dynamic injection model to yield a more realistic predicted peak pressure is crucial to improve the convergence of between the experimental and computed values of the heat release model. In addition to revising the inputs of the heat release model, there are other limitations that may affect the modeled domain and resulting convergence with experimental conditions. First, the model assumes infinitely fast mixing between the reactants, but the simulations from Nassini show that there is a distribution of equivalence ratio across a mixture [4]. In addition, the time scales of pre-deflagration are neglected and the resulting mixture is held frozen until passage of the detonation wave. Finally, the gases are ideal and so any non-ideal compressibility effects or changes in specific heat with temperature are ignored. Future developments will consider the time scales of the pre-deflagration process and mixing.

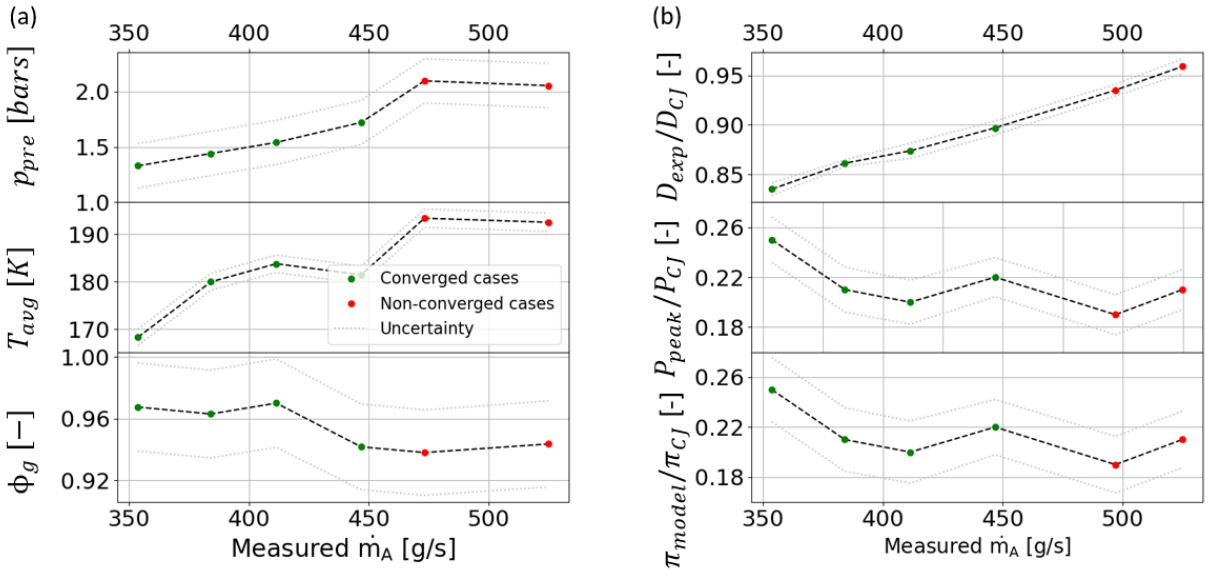

Fig. 14 (a) Variation of input parameters, namely, the pre-detonation pressure, average temperature and global equivalence ratio to the heat release model for different measured air mass flow rates, (b) Variation of the experimental wave speed, peak pressure and pressure ratio (computed from the dynamic inlet model) for measured air mass flow rates. These parameters are used to identify if there is a convergence on the calculated domain for a given experimental case.

IV. Conclusions

A low-order model has been developed to give insight on the detonation velocity deficit observed experimentally by accounting for the impact of non-ideal processes on key detonation properties. Three mechanisms are incorporated into the model: the buffer region created by non-premixed reactant injection, parasitic combustion of reactants and mixing with pre-detonation reactants, and reduction of the heat release through the detonation. The effect of these mechanisms reduces the heat release that supports the detonation wave and results in a reduction of detonation properties. By utilizing relatively easily measured experimental data as inputs, a parametric analysis was performed for stable single detonation runs on the RDC at TU Berlin. Convergence between predicted and experimental values reveal that a proportion of the heat release is lost in the buffer zone, pre-deflagrates or is unable to contribute to the detonation heat release. The lack of convergence for certain cases appears to be caused by a shortcoming of the dynamic injection model and the limitations of the temporal response of the pressure sensors, which under-predicts of the peak pressure and air injector blocked time. Improving the dynamic injection model to yield a more realistic predicted peak pressure is an on-going area of research. Future work will feature an extended parametric study to determine the impact of boundary conditions on characteristic parameters in the RDC. It is expected that varying the injector geometry will affect the injector response time and mixing, thereby modifying ψ and ω. In addition, changing the diameter of the inner annulus will impact the wall heat transfer, modifying the detonation heat release, χ.

Acknowledgments

This project has received funding from the European Union's Horizon 2020 research and innovation programme under the Marie Skłodowska-Curie grant agreement No 956803.

References

[1] Bach, E., Paschereit, C. O., Stathopoulos, P., and Bohon, M., "RDC Operation and Performance with Varying Air Injector Pressure Loss, AIAA Paper 2020-0199," January 2020.

[2] Bach, E., Stathopoulos, P., Paschereit, C. O., and Bohon, M. D., "Performance Analysis of a Rotating Detonation Combustor

Based on Stagnation Pressure Measurements," *Combustion and Flame*, Vol. 217, 2020, pp. 21–36.

[3] Klopsch, R., Garan, N., Bohon, M., Bach, E., Asli, M., and Stathopoulos, P., "2D Euler Modeling of Rotating Detonation Combustion in Preparation for Turbomachinery Matching, AIAA Paper 2023-1291," January 2022.

[4] Nassini, P. C., "High-fidelity numerical investigations of a hydrogen rotating detonation combustor," Phd thesis, University of Florence, 2022.

[5] Chacon, F., and Gamba, M., "Study of Parasitic Combustion in an Optically Accessible Continuous Wave Rotating Detonation Engine, AIAA Paper 2019-0473," January 2019.

[6] Sato, T., Chacon, F., White, L., Raman, V., and Gamba, M., "Mixing and detonation structure in a rotating detonation engine with an axial air inlet," *Proceedings of the Combustion Institute*, Vol. 38, No. 3, 2021, pp. 3769–3776.

[7] Fievisohn, R. T., Hoke, J., and Schumaker, S. A., "Product Recirculation and Incipient Autoignition in a Rotating Detonation Engine, AIAA Paper 2020-2286," January 2020.

[8] Strakey, P., Ferguson, D., Sisler, A., and Nix, A., "Computationally Quantifying Loss Mechanisms in a Rotating Detonation Engine, AIAA Paper 2016-0900," January 2016.

[9] Gaillard, T., Davidenko, D., and Dupoirieux, F., "Numerical simulation of a Rotating Detonation with a realistic injector designed for separate supply of gaseous hydrogen and oxygen," *Acta Astronautica*, Vol. 141, 2017, pp. 64–78.

[10] Davidenko, D., and Gaillard, T., "Injector Design Methodology Based on Computational Analysis of a Single Injection Element," *10th International Workshop on Detonation for Propulsion*, 2019.

[11] Lee, J. H. S., *The Detonation Phenomenon*, Cambridge University Press, 2008.

[12] Rankin, B. A., Fugger, C. A., Richardson, D. R., Cho, K. Y., Hoke, J., Caswell, A. W., Gord, J. R., and Schauer, F., "Evaluation of Mixing Processes in a Non-Premixed Rotating Detonation Engine Using Acetone PLIF, AIAA Paper 2016-1198," January 2016.

[13] Andrus, I. Q., King, P., Polanka, M. D., Schauer, F., and Hoke, J., "Experimentation of a Premixed Rotating Detonation Engine Utilizing a Variable Slot Feed Plenum, AIAA Paper 2016-1404," January 2016.

[14] Fievisohn, R. T., Hoke, J., and Holley, A., "Thermodynamic and Operability Implications of Product Recirculation in Rotating Detonation Engines, AIAA Paper 2019-4449," August 2019.

[15] Hansmetzger, S., Zitoun, R., and Vidal, P., "A study of continuous rotation modes of detonation in an annular chamber with constant or increasing section," *Shock Waves*, Vol. 28, No. 5, 2018, pp. 1065–1078.

[16] Stechmann, D. P., Sardeshmukh, S., Heister, S. D., and Mikoshiba, K., "Role of Ignition Delay in Rotating Detonation Engine Performance and Operability," *Journal of Propulsion and Power*, Vol. 35, No. 1, 2019, pp. 125–140.

[17] Feleo, A., Chacon, F., and Gamba, M., "Effects of Heat Release Distribution on Detonation Properties in a H2/Air Rotating Detonation Combustor from OH* Chemiluminesence, AIAA Paper 2019-4045," August 2019.

[18] Chacon, F., "Non-Ideal Phenomena in Rotating Detonation Combustors," Phd thesis, 2020.

[19] Kaemming, T., Fotia, M. L., Hoke, J., and Schauer, F., "Thermodynamic Modeling of a Rotating Detonation Engine Through a Reduced-Order Approach," *Journal of Propulsion and Power*, Vol. 33, No. 5, 2017, pp. 1170–1178.

[20] Bohon, M. D., Bluemner, R., Paschereit, C. O., and Gutmark, E. J., "High-speed imaging of wave modes in an RDC," *Experimental Thermal and Fluid Science*, Vol. 102, 2019, pp. 28–37.

[21] Shepherd, J. E., and Kasahara, J., "Analytical Models for the Thrust of a Rotating Detonation Engine," *GALCIT Report*, 2017.

[22] Bedick, C., Ferguson, D. H., and Strakey, P., "Validation and Application of a Reduced-Order Rotating Detonation Engine Inlet and Fill Zone Model, AIAA Paper 2021-0193," January 2021.

[23] White, F., *Fluid Mechanics*, McGraw Hill, 2011.

[24] Goodwin, D. G., Speth, R. L., Moffat, H. K., and Weber, B. W., "Cantera: An Object-oriented Software Toolkit for Chemical Kinetics, Thermodynamics, and Transport Processes," `https://www.cantera.org`, 2021.

[25] Sánchez, A. L., and Williams, F. A., "Recent advances in understanding of flammability characteristics of hydrogen," *Progress in Energy and Combustion Science*, Vol. 41, 2014, pp. 1–55.

[26] Browne, S., Ziegler, J., and Shepherd, J., "Shock and detonation toolbox," *GALCIT - Explosion Dynamics Laboratory*, 2008.

[27] Sato, T., Chacon, F., Gamba, M., and Raman, V., "Mass flow rate effect on a rotating detonation combustor with an axial air injection," *Shock Waves*, Vol. 31, No. 7, 2021, pp. 741–751.